Published version:

https://doi.org/10.1016/j.jlumin.2017.01.036

Judd–Ofelt modeling, emission lifetimes and non-radiative relaxation for Er^{3+} doped Cs_2NaYF_6 elpasolite crystals

P.A. Loiko[1], E.V. Vilejshikova[2], N.M. Khaidukov[3], J. Méndez-Ramos[4]
X. Mateos[5], and K.V. Yumashev[2,*]

[1]*ITMO University, 49 Kronverkskiy pr., St. Petersburg 197101, Russia*
[2]*Center for Optical Materials and Technologies (COMT), Belarusian National Technical University, 65/17 Nezavisimosti Ave., Minsk 220013, Belarus*
[3]*N.S. Kurnakov Institute of General and Inorganic Chemistry, 31 Leninskii Prospekt, Moscow 119991, Russia*
[4]*Departamento de Física, Universidad de La Laguna, La Laguna 38206, Tenerife, Spain*
[5]*Física i Cristal·lografia de Materials i Nanomaterials (FiCMA-FiCNA), Universitat Rovira i Virgili (URV), Campus Sescelades, c/ Marcel·lí Domingo, s/n., Tarragona 43007, Spain*

**Corresponding author e-mail: k.yumashev@tut.by*

Abstract. Absorption and emission properties of Er^{3+} ions in a cubic elpasolite crystal, Cs_2NaYF_6, are modeled within the Judd-Ofelt (J-O) theory. The J-O intensity parameters have been determined: Ω_2 = 0.665, Ω_4 = 0.217 and Ω_6 = 0.029 $\times 10^{-20}$ cm^2. The elpasolite structure of Cs_2NaYF_6 containing isolated [YF_6] polyhedra allows high Er^{3+} doping levels up to 100 at.% without considerable concentration quenching of luminescence and exceptionally long lifetimes of the excited states (in particular, the radiative lifetimes of the $^4I_{13/2}$ and $^4I_{11/2}$ states are as long as 36.7 ms and 113.4 ms, respectively). It also shows weak non-radiative relaxation. Stimulated-emission cross-sections have been determined for the Er^{3+} transitions in Cs_2NaYF_6 at ~2.7 and ~1.5 μm as well as in the visible spectral range.

Keywords: fluoride crystals; erbium; Judd-Ofelt analysis; stimulated emission

1. Introduction

During the past decade, fluoride crystals doped with rare-earth ions (RE^{3+}) have attracted a considerable attention for the development of solid-state lasers [1]. First, the fluorides possess low phonon energies ($h\nu_{max}$ ~350-500 cm^{-1}) [2]. This leads to weak non-radiative (NR) relaxation from the excited-states of the RE^{3+} ions [3] and, hence, long lifetimes τ, which is a key condition for low-threshold continuous-wave and high-pulse-energy Q-switched lasers [4]. Second, they possess large bandgap energies, E_g ~7-12 eV [5], which defines their excellent transparency in the UV and IR, as well as reduce the probability of multi-phonon absorption. Third, they show relatively low refractive index, n ~1.5 [6], and negative thermo-optic coefficients, dn/dT [7]. The latter compensates the effect of thermal expansion leading to weak thermal lensing [8]. Finally, the fluorides have typically high thermal conductivity [9].

Recently, crystals of cubic CaF_2, SrF_2, KY_3F_{10}, tetragonal $LiLnF_4$ (Ln = Y, Gd, Lu) and monoclinic BaY_2F_8 fluorides have been studied as laser hosts for doping with lanthanide ions such as Nd^{3+}, Yb^{3+}, Tm^{3+} or Ho^{3+} that emit at ~1 μm and at ~2 μm [1,4]. Particularly, for fluoride crystals, long upper laser level lifetimes result in the generation of high pulse energies in Q-switched lasers [10].

Trivalent erbium (Er^{3+}) ions possess an electronic configuration $[Xe]4f^{11}$ leading to a rich energy level structure of the 4f electrons. Within such a structure, a plurality of electronic transitions is detected and the transitions $^4I_{13/2} \rightarrow {}^4I_{15/2}$ and $^4I_{11/2} \rightarrow {}^4I_{13/2}$ at ~1.5 and ~2.7 μm, respectively, are frequently used for laser generation [11, 12]. On the other hand, such a structure supports various energy-transfer (ET) processes leading to upconversion and energy loss due to non-radiative transitions between the levels [13] by taking into account that the effect of upconversion is especially pronounced in fluoride materials [14]. One of the ways to eliminate such effects is to use a direct excitation to the upper laser level, the so-called in-band pumping scheme [15,16]. It should also be noted that a green laser due to upconversion in Er^{3+}-doped fluorides (the $^4S_{3/2} \rightarrow {}^4I_{15/2}$ transition, ~0.55 μm) has been developed [17]. The applicability of fluorides as hosts for various laser schemes is determined by the concentration of Er^{3+} ions because the probability of the ET processes is greatly dependent on the ion concentration [18].

The development of fluoride hosts is of interest for lasers because they may, simultaneously, allow for high RE^{3+} doping levels and show weak concentration quenching of the luminescence. The latter is caused by the low probability for ET between the optically active ions due to the structure features. Obviously such hosts should contain rare-earth ion polyhedra isolated from each other or isolated polyhedra groups. In particular, we studied previously [19] the spectroscopy of the orthorhombic fluoride Er^{3+}:K_2YF_5 having a chain structure.

In the present work, we focus on another complex fluoride, Er^{3+}:Cs_2NaYF_6 [20], belonging to the large family of cubic elpasolites, A_2BMX_6, where A and B are monovalent alkali cations, M is a trivalent metal ion and X is a halide anion [21]. In the elpasolite structure, the $[MX_6]$ polyhedra are perfect octahedra (O_h) and they don't share halogen ions [22]. Such a structure of Cs_2NaYF_6 with the isolated $[YF_6]$ octahedral units may provide small NR relaxation rates from excited states, very long lifetimes τ of these states [23,24] and the highest possible RE^{3+} (in particular Er^{3+}) doping levels up to the stoichiometric composition Cs_2NaErF_6 without considerable concentration quenching [20]. Thus, we provide here the results on Judd-Ofelt (J-O) analysis for the transition probabilities of Er^{3+} ions and a quantification for the NR relaxation in Cs_2NaYF_6, for the first time, to the best of our knowledge. To date, the crystal-field analysis of Er^{3+} in Cs_2NaYF_6 has been reported [25] and the decay time of the ~2.7 μm emission from Er^{3+} ions has been studied [24]. Recently, the data for optical absorption and the Stokes and anti-Stokes luminescence of Er^{3+} ions in Cs_2NaYF_6

have been presented [20]. It should be noted that there exist data for the spectral luminescence characteristics of Er^{3+} in chloroelpasolite Cs_2NaYCl_6 [26].

2. Crystal growth

Crystals of Cs_2NaYF_6 doped with Er^{3+} were grown under hydrothermal conditions. For the crystal growth, copper-insert lined autoclaves with a volume of ~40 cm^3 were utilized, and the inserts were separated by perforated diaphragms into synthesis and crystallization zones. The crystals were synthesized by a direct temperature-gradient method as a result of a reaction of aqueous solutions containing 35–40 mol% CsF and 8–10 mol% NaF with oxide mixtures $(1-x)Y_2O_3 – xEr_2O_3$ (purity: 99.99%) where x = 0.003, 0.03, 0.1 and 1 at a temperature of ~750 K in the synthesis zone, temperature gradient along the reactor body of up to 3K/cm, and pressure of ~100 MPa. Spontaneously nucleated crystals of up to 0.5 cm^3 were grown in the upper crystallization zone of the autoclave for 200 h. The crystals were transparent and had slight rose coloration due to the Er^{3+} dopant. No annealing treatment of the as-grown crystals was performed.

The structure and the phase purity of the grown crystals have been studied by X-ray powder diffraction analysis (XRD). The Cs_2NaYF_6 crystal synthesized under hydrothermal conditions crystallizes in the cubic system, sp. gr. Fm3m, a = 9.057 Å, Z = 4, density ρ = 4.42 g/cm^3. Therefore, in the Cs_2NaYF_6 elpasolite structure there is one crystallographic site for Y^{3+} ions which is VI-fold coordinated by the F^- ions forming the perfect octahedron and its structure is shown in Fig. 1. The shortest Y^{3+}-Y^{3+} distance along the ***c***-axis is 9.0496 Å and in the ***a***-***b*** plane, it is 6.3990 Å. It should be noted that fluoroelpasolite Cs_2NaErF_6 has almost the same lattice parameters, which allow obtaining Cs_2NaYF_6 crystals where the Er^{3+} concentrations correspond to those of the starting oxide mixtures $(1-x)Y_2O_3 – xEr_2O_3$ (Table 1).

3. Experimental

The spectral properties of Er^{3+}:Cs_2NaYF_6 crystals were studied with unpolarized light at room-temperature (RT, 293 K) by taking into account that the cubic fluoroelpasolite crystals are optically isotropic. Also they possess a wide band-gap (E_g ~6.9 eV) [27].

The absorption spectra were measured for a 10 at.% Er^{3+}:Cs_2NaYF_6 crystal, 1 mm-thick polished plate by using a Varian CARY-5000 spectrophotometer with a spectral bandwidth (SBW) of 0.02 nm. The absorption cross-sections, σ_{abs}, were derived as α/N_{Er}, where α was the absorption coefficient and $N_{Er} = 5.38\times10^{20}$ at/cm^3 was the Er^{3+} concentration.

The emission spectra were measured for a 10 at.% Er:Cs_2NaYF_6 crystal under CW excitation by a 960 nm InGaAs laser diode directly to the $^4I_{11/2}$ state. For the registration of the green and the ~1.5 μm luminescence, a lock-in amplifier (Stanford Research Systems, model SR810), a grating monochromator MDR-23 (SBW = 0.1 nm) and a G5851 Hamamatsu InGaAs PIN photodiode (for near-IR) or an APD module C5460-01 (for visible) were used. The luminescence was collected with a wide-aperture lens. For the ~2.7 μm luminescence, a compact Fourier transform infrared spectrometer, model FT-IR Rocket from Arcoptix, was used. It was equipped with an optical fiber for luminescence collection.

The luminescence decay was studied under quasi-CW excitation at 960 nm in the same set-up. The diode output was mechanically chopped (cut-off time: 5 μs) at a frequency of ~16 Hz by using a 500 MHz Textronix TDS-3052B digital oscilloscope monitoring the luminescence decay curves at 0.55 μm (from the $^4S_{3/2}$ state), at 0.66 μm ($^4F_{9/2}$ state), at 0.82 μm ($^4I_{9/2}$ state), at 1.0 μm ($^4I_{11/2}$ state) and at 1.55 μm ($^4I_{13/2}$ state). For the last two wavelengths, the samples of Cs_2NaYF_6 containing 0.3, 3, 10 and 100 at.% Er^{3+} were studied and for the visible emissions, only a 0.3 at.% Er^{3+} doped Cs_2NaYF_6 was investigated. To

avoid radiation trapping effects, the samples were powdered and immersed in glycerin (5-10 wt.% of powder). The decay curves were fitted according to a single-exponential law, $I(t) = I_0\exp(-t/\tau_{exp})$.

4. Results and discussion

3.1 Optical absorption

The absorption spectrum of a 10 at.% Er:Cs_2NaYF_6 crystal within the 0.35-1.65 μm spectral range at RT is shown in Fig. 2. The absorption bands are related to the transitions from the $^4I_{15/2}$ ground-state to the excited states indicated in Fig. 3, showing the scheme of energy-levels for Er^{3+} in Cs_2NaYF_6, according to [25]. For the $^4I_{15/2} \rightarrow {}^4I_{13/2}$ transition, the maximum σ_{abs} is 4.6×10^{21} at 1532 nm (case of in-band pumping) and for the $^4I_{15/2} \rightarrow {}^4I_{11/2}$ one, the maximum σ_{abs} is considerably lower being 0.07×10^{21} at 963 nm.

The absorption spectrum is analyzed within the standard Judd-Ofelt (J-O) theory [28, 29]. In this case the absorption oscillator strengths f_{exp} have been determined from the measured absorption spectra as:

$$f_{\Sigma}^{\exp}(JJ') = \frac{m_e c^2}{\pi e^2 N_{\mathrm{Er}} \langle\lambda\rangle^2}\Gamma(JJ'), \quad (1)$$

where m_e and e are the electron mass and its charge, respectively, c is the speed of light, Γ(JJ') is the integrated absorption coefficient within the absorption band and ‹λ› is the "center of gravity" of the absorption band.

It should be noted that the J-O theory describes electric-dipole (ED) transitions. The contribution of magnetic-dipole (MD) transitions corresponding to J–J' = 0, ±1 (f_{MD}) can be found in research publications, for example in [30]. Based on the experimental ED absorption oscillator strengths, the line strengths have been derived:

$$S_{ED}^{\exp}(JJ') = \frac{3h(2J'+1)\langle\lambda\rangle}{8}\frac{9n}{(n^2+2)^2} f_{ED}^{\exp}(JJ'). \quad (2)$$

Here, h is the Planck constant and n is the refractive index of the crystal. The set of experimental ED line strengths is fitted as:

$$S_{ED}^{calc}(JJ') = \sum_{k=2,4,6} U^{(k)}\Omega_k, \quad (3a)$$

$$U^{(k)} = \langle(4f^n)SLJ\|U^k\|(4f^n)S'L'J'\rangle^2. \quad (3b)$$

Here, $U^{(k)}$ are the squared reduced matrix elements [31] and Ω_k, k = 2, 4, 6, are the J-O intensity parameters. Accordingly, the absorption oscillator strengths are:

$$f_{\Sigma}^{calc}(JJ') = \frac{8}{3h(2J'+1)\langle\lambda\rangle}\frac{(n^2+2)^2}{9n} S_{\mathrm{ED}}^{calc}(JJ') + f_{\mathrm{MD}}(JJ'). \quad (4)$$

The results on ‹λ›, Γ, f_{exp} and f_{calc} for 10 at.% Er^{3+}:Cs_2NaYF_6 are summarized in Table 2. The root-mean-square (RMS) deviation between the experimental and calculated absorption oscillator strengths is 0.208. The determined J-O parameters are: Ω_2 = 0.665, Ω_4 = 0.217 and Ω_6 = 0.029 $\times10^{-20}$ cm^2. In addition, the Ω_k parameters for Er^{3+}:Cs_2NaYF_6 in comparison with those for various Er^{3+}-doped fluoride crystals, oxyfluoride glass and ensuing glass-ceramics (GC) [3,32-38] are presented in Table 3. As one can see, the J-O parameters for Er^{3+}:Cs_2NaYF_6 are lower than those for the previously studied fluoride hosts. This is because of a relatively small transition probability between the Er^{3+} levels in this structure, caused by the highly symmetrical octahedral environment.

3.2 Emission and radiative lifetimes

The determined J-O parameters have been used to calculate the emission probabilities of the Er^{3+} ions in Cs_2NaYF_6. The probabilities of spontaneous radiative transitions are calculated as:

$$A_{\Sigma}^{calc}(JJ') = \frac{64\pi^4 e^2}{3h(2J'+1)\langle\lambda\rangle^3} n\left(\frac{n^2+2}{3}\right)^2 S_{\mathrm{ED}}^{calc}(JJ') + A_{\mathrm{MD}}(JJ').\cdot \quad (5)$$

Here, the first term accounts for ED transitions and it is related to the line strength of the J → J' transition determined by Eq. (3a), whereas the set of squared reduced matrix elements $U^{(k)}$ for emission transitions can be found elsewhere [31], and the second term accounts for MD transitions [30].

Using the probabilities of the spontaneous radiative transitions for separate emission channels J→J', we have calculated the total probabilities A_{tot}, the corresponding radiative lifetimes of the excited-states τ_{rad} and the luminescence branching ratios for the emission channels B(JJ'):

$$\tau_{rad} = \frac{1}{A_{tot}^{calc}}, \text{ where } A_{tot}^{calc} = \sum_{J'} A_{\Sigma}^{calc}(JJ'), \quad (6a)$$

$$B(JJ') = \frac{A_{\Sigma}^{calc}(JJ')}{\sum_{J'} A_{\Sigma}^{calc}(JJ')}. \quad (6b)$$

The results are summarized in Table 4 for the excited states with levels from $^4I_{13/2}$ to $^4G_{11/2}$. However, it should be noted that only the transitions corresponding to branching ratios B(JJ') > 0.01 (1%) are listed. Based on the multiplet barycenters [25], we have determined the average emission wavelengths for each transition ‹λ›. The radiative lifetimes of the $^4I_{13/2}$ and $^4I_{11/2}$ states of Er^{3+} ions in Cs_2NaYF_6 are as long as 36.7 ms and 113.4 ms, respectively, which are outstanding compared with the known Er^{3+}-doped oxide and fluoride laser crystals, oxyfluoride glass and GC, Table 5. The τ_{rad} values for Er^{3+}:Cs_2NaYF_6 are even longer than those for the previously studied Er^{3+}:K_2YF_5 crystal in which the [(Y/Er)F_7] polyhedra form isolated chains and the intrachain Y^{3+}-Y^{3+} distances are about ~3.7 Å [32].

3.3 Luminescence decay measurements

To confirm the exceptionally long lifetimes of Er^{3+} ions in Cs_2NaYF_6, we have studied the luminescence decay from the $^4I_{13/2}$ and $^4I_{11/2}$ states for various Er^{3+} doping levels ranging from 0.3 at.% to 100 at.% i.e. for a stoichiometric Cs_2NaErF_6 crystal. The results are shown in Fig. 4 where the decay curves are plotted in a semi-log scale. The decay curves are single-exponential. This agrees well with the existence of a single site for Er^{3+} ions in the elpasolite structure. For a 0.3 at.% Er^{3+}:Cs_2NaYF_6 crystal in which the effect of concentration-quenching is almost negligible, the measured lifetime τ_{exp} of the $^4I_{13/2}$ state is 34.5 ms and $\tau_{exp}(^4I_{11/2})$ is 14.1 ms. The experimental lifetime of the $^4I_{13/2}$ state is very close to the radiative one determined from the J-O calculations, so the luminescence quantum efficiency (τ_{exp}/τ_{rad}) η_q is equal to 94%. Such a value indicates weak NR relaxation from this state, caused, on the one hand, by the large energy-gap between this state and the ground-state (ΔE = 6506 cm^{-1}) compared to $h\nu_{max}$ = 468 cm^{-1} [42] and, on the other hand, by the high optical quality of the crystal and high crystallinity of its structure. The experimental lifetime of the $^4I_{11/2}$ state is shorter than the radiative one, which is typical for Er^{3+} ions and is attributed to much stronger NR relaxation from this state to the lower-lying $^4I_{13/2}$ one due to the smaller energy-gap (ΔE = 3889 cm^{-1}, see details below). The concentration-quenching of luminescence for 10 at.% Er^{3+} doped crystal is very modest, as $\tau_{exp}(^4I_{13/2})$ = 27.6 ms and $\tau_{exp}(^4I_{11/2})$ = 11.9 ms. For the stoichiometric Cs_2NaErF_6 crystal, this effect is more pronounced but the lifetimes still remain within the ms-range, 10.5 ms and 2.72 ms, respectively.

The observed behavior of τ_{exp} versus N_{Er} indicates extremely weak energy excitation transfer between Er^{3+} ions in the Cs_2NaYF_6 lattice. The concentration quenching of the luminescence from the $^4I_{13/2}$ level is attributed to the energy-migration (donor-donor energy transfer) among the Er^{3+} ions by taking into account that the probability of this process is concentration-dependent [43]. The shortening of the $^4I_{11/2}$ lifetime is due to several energy-transfer upconversion (ETU) processes, namely donor-acceptor interactions, some of which are phonon-assisted, leading to the depopulation of this state [44]. The probabilities of ETU processes are also concentration-dependent.

It should be emphasized that only the experimental lifetimes for the $^4I_{11/2}$ state of Er^{3+} in Cs_2NaYF_6 have been reported [24], namely ~12±2 ms for 1 at.% Er^{3+} doping and ~0.7±2 ms for Cs_2NaErF_6, which agree well with our data.

3.4 Stimulated-emission cross-sections

The determined radiative lifetimes τ_{rad} of the excited states allow one to calculate the stimulated-emission (SE) cross-sections, σ_{SE}, for the transitions of interest for laser applications, Fig. 3, namely $^4I_{13/2} \rightarrow {}^4I_{15/2}$ (emission at ~1.5 μm), $^4I_{11/2} \rightarrow {}^4I_{13/2}$ (at ~2.7 μm) and $^4S_{3/2} \rightarrow {}^4I_{15/2}$ (at ~0.55 μm). For all these transitions, we have used the Füchtbauer–Ladenburg (F-L) equation [45]:

$$\sigma_{SE}(\lambda)=\frac{\lambda^5}{8\pi n^2 \tau_{rad} c}\frac{W(\lambda)B(JJ')}{\int \lambda W(\lambda)\mathrm{d}\lambda}. \quad (7)$$

Here, $W(\lambda)$ is the measured luminescence spectrum for the considered J→J' transition, corrected for the response of the photodetector. For the $^4I_{13/2} \rightarrow {}^4I_{15/2}$ transition, due to the overlap of the absorption and emission bands, the measured $W(\lambda)$ is strongly affected by reabsorption. Thus, one may use the reciprocity method [46] as an alternative approach:

$$\sigma_{SE}(\lambda)=\sigma_{abs}(\lambda)\frac{Z_1}{Z_2}\exp\left(-\frac{hc/\lambda - E_{ZL}}{kT}\right), \quad (8a)$$

$$Z_m=\sum_k g_k^m \exp(-E_k^m/kT), \quad (8b)$$

where $\sigma_{abs}(\lambda)$ is the absorption cross-section spectrum for the corresponding J'→J transition, k is the Boltzmann constant, T is the crystal temperature (RT), Z_m are the partition functions the lower (m = 1) and upper (m =2) multiplets, $\{E^m_k\}$ is the set of energies of the Stark sub-levels of the two multiplets measured from the lower sublevel of the multiplet, g^m_k is the degeneration of the sub-level with the number k and energy E^m_k, and E_{ZL} is the energy difference between the lowest Stark sub-levels of the two multiplets (zero-phonon line). The energies of the Stark sub-levels for Er^{3+} in the elpasolite structure can be found elsewhere [25].

The results on the SE cross-sections for Er^{3+}:Cs_2NaYF_6 are shown in Fig. 5. For the $^4I_{13/2} \rightarrow {}^4I_{15/2}$ transition, the maximum σ_{SE} is 3.78×10^{-21} cm^2 at 1535.3 nm. More details about this transition, in particular the gain spectra, can be found in [20]. An additional comparison can be made with corresponding reported values for the 2.7 μm emission in Er^{3+}-doped oxyfluoride glass and ensuing GC [47]. For the $^4I_{11/2} \rightarrow {}^4I_{13/2}$ transition, the emission in the 2.67–2.9 μm spectral range is shown in Fig. 5(b). This agrees with the range expected from the Stark structure of the involved multiplets, 3430–3744 cm^{-1}. The emission band contains two intense peaks at 2705.0 nm (σ_{SE} = 2.60×10^{-21} cm^2) and at 2855.2 nm (σ_{SE} = 2.97×10^{-21} cm^2). Such a spectral behavior is explained by the large splitting of the $^4I_{11/2}$ multiplet (72 cm^{-1}) containing 4 Stark sub-levels, two of which are closely located [25]. The first peak is attributed to the $\Gamma_6 + a\Gamma_8 \rightarrow \Gamma_6$ transition from the lower-lying Stark sub-levels, and the second one to the $\Gamma_7 + b\Gamma_8 \rightarrow \Gamma_6$ transition from the upper-lying sub-levels. The results for the $^4S_{3/2} \rightarrow {}^4I_{15/2}$ transition are presented in Fig. 5(c). The corresponding

emission band contains some local peaks at 548.3 nm, 554.7 nm and 563.6 nm and the maximum σ_{SE} is 1.18×10^{-22} cm^2 corresponding to the last local peak. The determined σ_{SE} values are much lower than those for the previously studied Er^{3+}:K_2YF_5 [32] due to much longer radiative lifetimes.

3.5 Non-radiative relaxation

The quantification of NR relaxation in laser materials is important for the prediction of the experimental lifetimes for the excited states of the RE^{3+} ions [3]. In this context, a 0.3 at.% Er^{3+} doped Cs_2NaYF_6 crystal has been selected to determine the NR relaxation rates A_{NR}. As for such a low concentration, the effect of various ET processes on the shortening of the experimental lifetime is negligible [43]. In this case the values of τ_{exp} have been measured for the excited-states $^4I_{13/2}$, $^4I_{11/2}$, $^4I_{9/2}$, $^4F_{9/2}$ and $^4S_{3/2}$, see Table 6. Accordingly, the A_{NR} is estimated from τ_{exp} and the total rate of spontaneous radiative transitions is estimated from the excited state, derived from J-O modeling (cf. Table 4) [40]:

$$A_{\mathrm{NR}}^{\mathrm{exp}}(JJ')=(1/\tau_{\mathrm{exp}})-A_{\Sigma}^{calc}(JJ'). \quad (9)$$

Theoretically, A_{NR} is represented as [3]:

$$A_{\mathrm{NR}}^{calc}(JJ')=Ce^{-\alpha\Delta E(JJ')}. \quad (10)$$

Here, C and α are the constants defined at a certain temperature which are characteristic for a specific material and ΔE is the energy-gap to the lowest excited-state. C has the meaning of the non-radiative relaxation rate in the limit of the zero energy gap and $\alpha = -\ln(\varepsilon)/h\nu_{ph}$ where ε is the ratio between probabilities of m-phonon and m-1-phonon relaxation and $h\nu_{ph}$ is the phonon energy. The results of the calculations for A_{NR} are presented in Table 6 and the experimental data on A_{NR} as well as their fit with Eq. (10) yielding C and α constants are shown in Fig. 6. The fit yields $C = 2.78\times10^7$ s^{-1} and $\alpha = 1.31\times10^{-3}$ cm which are relatively low values taking into account the data in Table 7 showing the values of C, α and $h\nu_{max}$ for various fluoride crystals.

4. Conclusion

We report on the Judd-Ofelt modeling of the absorption and emission properties for Er^{3+} ions in a cubic elpasolite Cs_2NaYF_6 crystal. The specific structure of this optical material containing isolated [(Y/Er)F_6] polyhedra and providing large Y^{3+}-Y^{3+} distances (6.4 – 9.05 Å), as well as a relatively small maximum phonon energy, 468 cm^{-1}, results in exceptionally long lifetimes of the excited-states and weak concentration quenching of the luminescence. The stimulated-emission cross-sections for the different transitions of Er^{3+} ions in the visible (green) and near-IR (at ~1.5 μm and at ~2.7 μm) ranges are evaluated giving rise to the obtained σ_{SE} values ranging from 1.18×10^{-22} cm^2 at 563.6 nm to 3.78×10^{-21} cm^2 at 1535.3 nm, 2.60×10^{-21} cm^2 at 2705.0 nm and 2.97×10^{-21} cm^2 at 2855.2 nm. The non-radiative relaxation from the excited-states of Er^{3+} ions is quantified.

Rare-earth doped, in particular, Er^{3+}-doped, cubic elpasolite Cs_2NaYF_6 crystals are promising optical materials for applications in up- and down-conversion materials [20]. The results of the present study indicate that Cs_2NaYF_6 crystals containing Er^{3+} may be considered for producing low-threshold eye-safe lasers emitting at ~1.7 μm and 2.7 μm. For this purpose, the growth technology of large crystals should be developed. On the other hand, further spectroscopic research on this material should focus on the optimization of the Er^{3+} concentration in Cs_2NaYF_6 by basing on the quantification of the ETU micro-parameters.

Acknowledgments

This research was partially supported by the Russian Foundation for Basic Research, research project No. 15-03-02507a and the Federal Agency of Scientific Organizations

within the State Assignment on Fundamental Research to the Kurnakov Institute of General and Inorganic Chemistry (IGIC RAS). Project MAGEC (Materials for Advanced Generation of Energy at Canary Islands) was supported by "Fundación Cajacanarias", and the Spanish Ministry of Economy and Competitiveness (projects ENE2013-47826-C4-4-R and ENE2016-74889-C4-2-R). P. Loiko acknowledges financial support from the Government of the Russian Federation (Grant 074-U01) through ITMO Post-Doctoral Fellowship scheme.

References

1. A. A. Kaminskii, Laser & Photon. Rev. 1 (2007) 93-177.
2. J. L. Doualan and R. Moncorgé, Ann. Chim. Sci. Mat. 28 (2003) 5–20.
3. M. J. Weber, Phys. Rev. 157 (1967) 262–272.
4. R. Moncorgé, A. Braud, P. Camy, J. L. Doualan, Fluoride laser crystals, *in Handbook of Solid-State Lasers*, B. Denker and E. Shklovsky, Eds. P. 28-53 (2013).
5. J. C. Krupa, M. Queffelec, J. Alloys Comp. 250 (1997) 287-292.
6. M. Daimon, A. Masumura, Appl. Opt. 41 (2002) 5275-5281.
7. W. J. Tropf, Opt. Eng. 34 (1995) 1369-1373.
8. P. J. Hardman, W. A. Clarkson, G. J. Friel, M. Pollnau, D. C. Hanna, IEEE J. Quant. Electron. 35 (2002) 647-655.
9. R. L. Aggarwal, D. J. Ripin, J. R. Ochoa, T. Y. Fan, J. Appl. Phys. 98 (2005) 103514-1-14.
10. H. Yu, V. Petrov, U. Griebner, D. Parisi, S. Veronesi, M. Tonelli, Opt. Lett. 37 (2012) 2544-2546.
11. G. Karlsson, F. Laurell, J. Tellefsen, B. Denker, B. Galagan, V. Osiko, S. Sverchkov, Appl. Phys. B 75 (2002) 41-46.
12. B. J. Dinerman, P. F. Moulton, Opt. Lett. 19 (1994) 1143-1145.
13. S. R. Lüthi, M. Pollnau, H. U. Güdel, M. P. Hehlen, Phys. Rev. B 60 (1999) 162-178.
14. Y. Wang, J. Ohwaki, Appl. Phys. Lett. 63 (1993) 3268-3270.
15. J. O. White, M. Dubinskii, L. D. Merkle, I. Kudryashov, D. Garbuzov, J. Opt. Soc. Am. B 24 (2007) 2454-2460.
16. K. N. Gorbachenya, S. V. Kurilchik, V. E. Kisel, A. S. Yasukevich, N. V. Kuleshov, A. S. Nizamutdinov, S. L. Korableva, V. V. Semashko, Quantum Electron. 46 (2016) 95-99.
17. R. Brede, E. Heumann, J. Koetke, T. Danger, G. Huber, B. Chai, Appl. Phys. Lett. 63 (1993) 2030–2031.
18. P. Loiko, M. Pollnau, J. Phys. Chem. C 120 (2016) 26480-26489.
19. P. A. Loiko, N. M. Khaidukov, J. Méndez-Ramos, E. V. Vilejshikova, N. A. Skoptsov, K. V. Yumashev, J. Lumin. 170 (2016) 1-7.
20. P. A. Loiko, N. M. Khaidukov, J. Méndez-Ramos, E. V. Vilejshikova, N. A. Skoptsov, K. V. Yumashev, J. Lumin. 175 (2016) 260–266.
21. G. Meyer, Prog. Sol. St. Chem. 14 (1982) 141–219.
22. L. R. Moras, J. Inorg. Nucl. Chem. 36 (1974) 3876–3878.
23. D. S. Pytalev, A. Jaffres, P. Aschehoug, P. A. Ryabochkina, A. V. Malov, N. M. Khaidukov, M. N. Popova, J. Lumin. 153 (2014) 125–129.
24. H. Vrielinck, I. Izeddin, V.Y. Ivanov, T. Gregorkiewicz, F. Callens, D.S. Lee, A.J. Steckl, N. M. Khaidukov, Mater. Res. Soc. Symp. 866 (2005) V381–V386.
25. X. Zhou, P. A. Tanner, M. D. Faucher, J. Phys. Chem. C 111 (2007) 683–687.
26. Mazurak, E. Lujowiak, B. Jezowska-Trzebiatowska, W. Ryba-Romanowski, J. Lumin. 29 (1984) 47–53.
27. M. G. Brik, V. Krasnenko, P. A. Tanner, J. Lumin. 152 (2014) 49–53.
28. B. R. Judd, Phys. Rev. 172 (1962) 750–761.
29. G. S. Ofelt, J. Chem. Phys. 37 (1962) 511–519.

30. C. M. Dodson, R. Zia, Phys. Rev. B 86 (2012) 125102-1-10.
31. A. A. Kaminskii, V. S. Mironov, A. Kornienko, S. N. Bagaev, G. Boulon, A. Brenier, B. Di Bartolo. Phys. Stat. Sol. (a),151 (1995) 231-255.
32. P. A. Loiko, E. V. Vilejshikova, N. M. Khaidukov, M. N. Brekhovskikh, X. Mateos, M. Aguiló, K. V. Yumashev, J. Lumin. 180 (2016) 103-110.
33. A. M. Tkachuk, S. É. Ivanova, M. F. Joubert, Y. Guyot, Opt. & Spectr. 97 (2004) 251-269.
34. C. Li, Y. Zhang, X. Zhang, D. Miao, H. Lin, M. Tonelli, F. Zeng, J. Liu, Mater. Sci. Appl. 2 (2011) 1161–1165.
35. A. Baraldi, R. Capelletti, M. Mazzera, A. Ponzoni, G. Amoretti, N. Magnani, A. Toncelli, M. Tonelli, Phys. Rev. B 72 (2005) 075132.
36. D. N. Patel, R. B. Reddy, S. K. Nash-Stevenson, Appl. Opt. 37 (1988) 7805–7808.
37. E. Preda, M. Stef, G. Buse, A. Pruna, I. Nicoara, Phys. Scripta 79 (2009) 035304.
38. J. Méndez Ramos, V. Lavín, I.R. Martín, U. R. Rodríguez-Mendoza, J. A. González-Almeida, V. D. Rodríguez, A. D. Lozano-Gorrín, P. Núñez, J. Alloy Compd 323–324 (2001) 753–758.
39. A. A. Kaminski, A. G. Petrosyan, G. A. Denisenko, T. I. Butaeva, V. A. Fedorov, S. E. Sarkisov, Phys. Stat. Sol. (a) 71 (1982) 291–312.
40. P. A. Loiko, E. A. Arbabzadah, M. J. Damzen, X. Mateos, E. B. Dunina, A. A. Kornienko, A. S. Yasukevich, N. A. Skoptsov, K. V. Yumashev, J. Lumin. 171 (2016) 226–273.
41. M. Pollnau, R. Spring, Ch. Ghisler, S. Wittwer, W. Luthy, H.P. Weber, IEEE J. Quantum Electron. 32 (1996) 657.
42. P.A. Tanner, Y.L. Liu, N. Edelstein, K. Murdoch, N.M. Khaidukov, J. Phys.: Condens. Matter 9 (1997) 7817–7836.
43. L. Agazzi, K. Wörhoff, M. Pollnau, J. Phys. Chem. C 117 (2013) 6759−6776.
44. L. Agazzi, K. Wörhoff, A. Kahn, M. Fechner, G. Huber, M. Pollnau, J. Opt. Soc. Am. B 30 (2013) 663-677.
45. S.A. Payne, L.L. Chase, L.K. Smith, W.L. Kway, W.F. Krupke, IEEE J. Quant. Electron. 28 (1992) 2619–2630.
46. B.F. Aull, H.P. Jenssen, IEEE J. Quantum Electron. 18 (1982) 925–930.
47. L. A. Riseberg, M.J. Weber, Progr. Opt. 14 (1977) 89-159.
48. V. K. Tikhomirov, J. Méndez-Ramos, V. D. Rodríguez, D. Furniss, A. B. Seddon, Opt. Mater. 28 (2006) 1143-1146.
49. J. M. Flaherty, B. Di Bartolo, J. Lumin. 8 (1973) 51-70.
50. L.A. Riseberg, H.W. Moos “Multiphonon orbit-lattice relaxation of excited states of rare-earth ions in crystals”. Physical Review. 174.2 (1968) 429.
51. L. F. Johnson, H. J. Guggenheim, Appl. Phys. Lett. 23 (1973) 96-98.

Figure captions

Figure 1. Unit-cell structure of Er:Cs_2NaYF_6 crystal, green polyhedra show the $[(Y/Er)F_6]^{3-}$ groups.

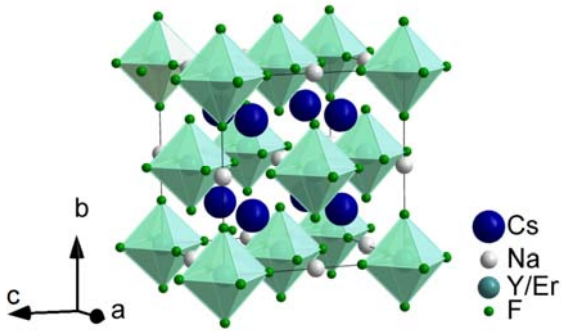

Figure 2. Absorption cross-section, σ_{abs}, spectrum of a 10 at.% Er^{3+}:Cs_2NaYF_6 crystal.

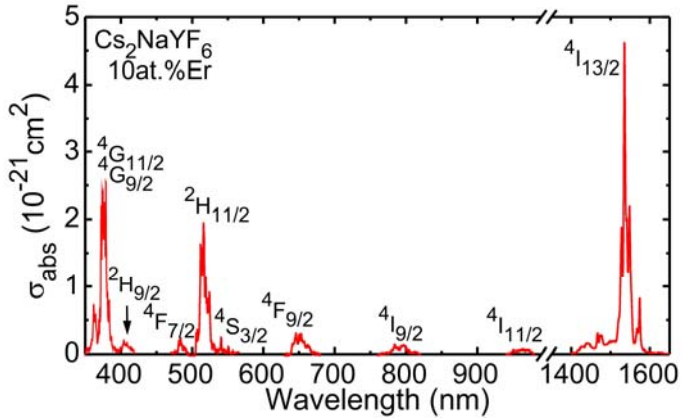

Figure 3. Energy level scheme of Er^{3+} ions in Cs_2NaYF_6, according to [25], *arrows* indicate relevant processes.

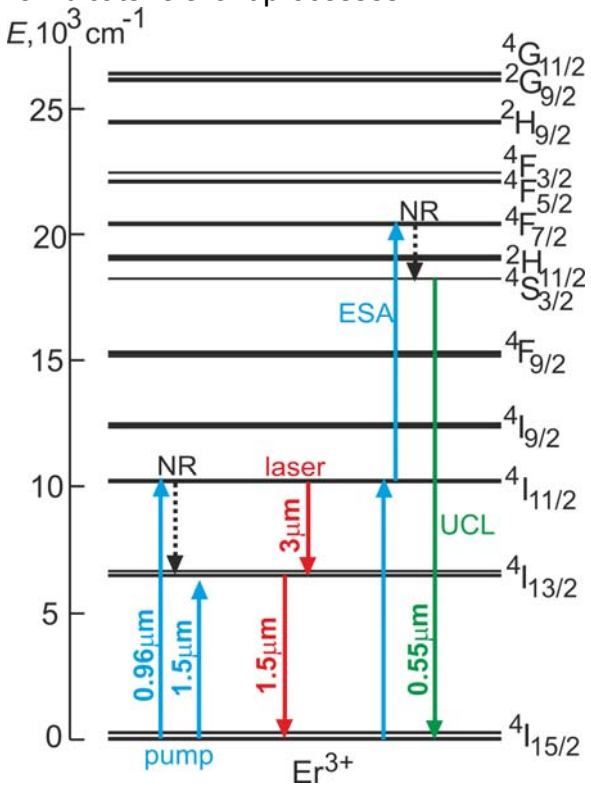

Figure 4. Luminescence decay curves from the $^4I_{13/2}$ (a) and $^4I_{11/2}$ (b) excited states of Er^{3+} ions in Cs_2NaYF_6 for various doping levels; λ_{exc} = 970 nm, λ_{lum} = 1540 nm (a) or 1000 nm (b).

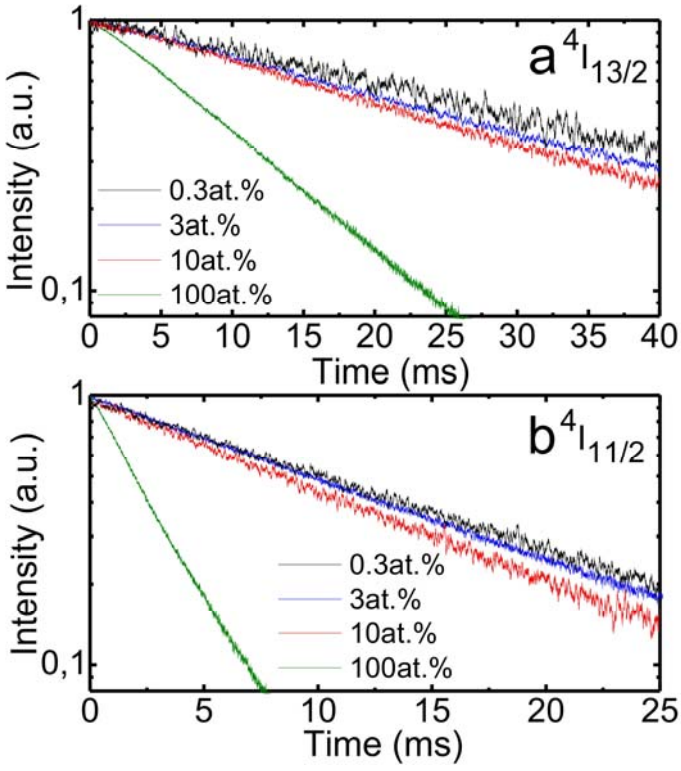

Figure 5 Stimulated-emission cross-section, σ_{SE}, spectra for the $^4I_{13/2} \rightarrow {}^4I_{15/2}$ (a), $^4I_{11/2} \rightarrow {}^4I_{13/2}$ (b) and $^4S_{3/2} \rightarrow {}^4I_{15/2}$ (c) transitions of Er^{3+} ions in a Cs_2NaYF_6 crystal, as calculated with the reciprocity and Füchtbauer–Ladenburg (F–L) methods.

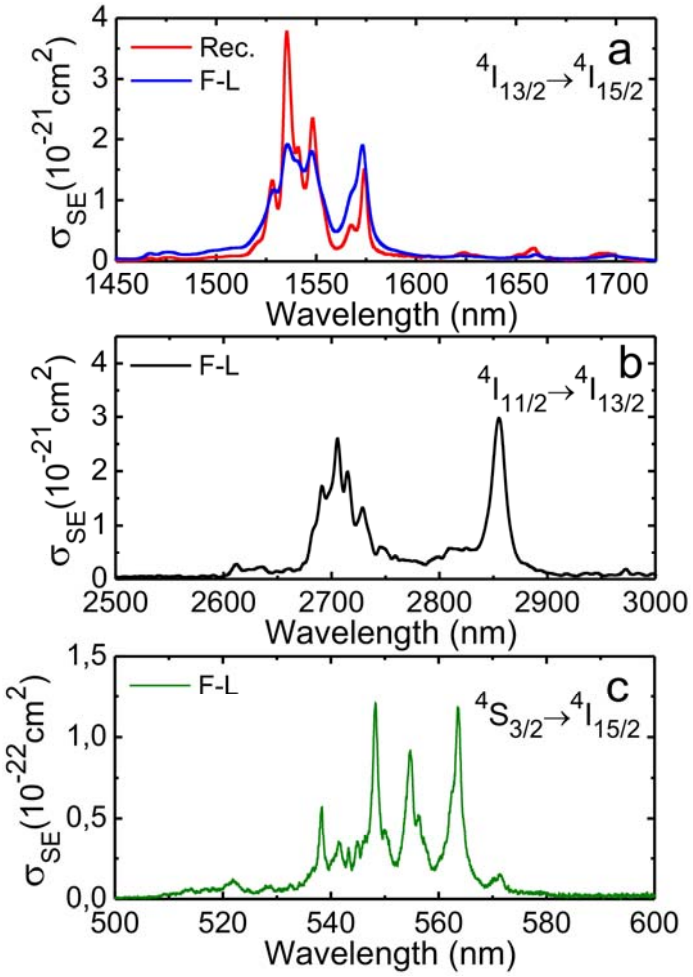

Figure 6 Energy-gap dependence of the nonradiative decay-rate constants A_{NR} in a 0.3 at.% Er^{3+}:Cs_2NaYF_6 crystal: *circles* are the values determined from the measured luminescence lifetimes and the calculated radiative decay rate constants, *line* is the fit of these data with Eq. (10).

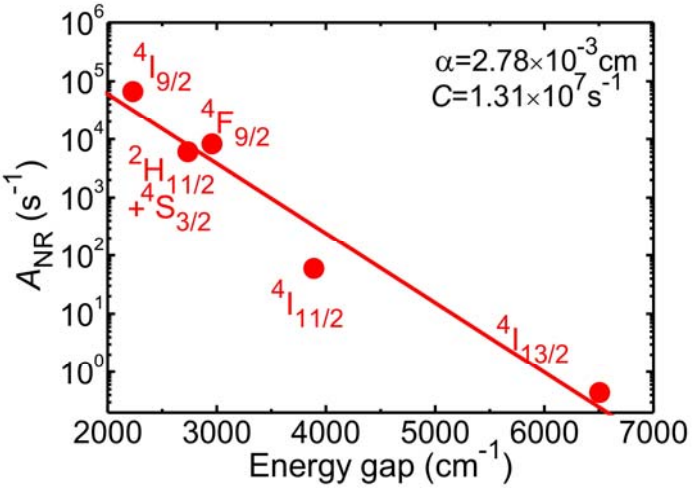

Table 1. Lattice parameter (a), unit cell volume (V), calculated density (ρ) and absolute concentration of Er^{3+} ions (N_{Er}) for cubic elpasolites (space group: Fm3m, $Z = 4$).

Crystal	a, Å	V, Å^3	ρ, g/cm^3	N_{Er}, at/cm^3
Cs_2NaYF_6	9.0496	741.12	4.405	-
$Cs_2NaY_{0.997}Er_{0.003}F_6$	9.0496	741.12	4.405	1.62×10^{19}
$Cs_2NaY_{0.97}Er_{0.03}F_6$	9.0492	741.02	4.427	1.62×10^{20}
$Cs_2NaY_{0.9}Er_{0.1}F_6$	9.0485	740.85	4.481	5.40×10^{20}
Cs_2NaErF_6	9.0411	739.03	5.122	5.41×10^{21}

Table 2. Experimental f_{exp} and calculated f_{calc} absorption oscillator strengths for a 10 at.% Er^{3+}:Cs_2NaYF_6 crystal.

Transition, $^4I_{15/2}\rightarrow$	‹λ›, nm	Γ, nm×cm^{-1}	f_{exp}, 10^{-7}	f_{calc}, 10^{-7}
$^4I_{13/2}$	1537.0	51.19	4.550	$0.421^{ED}+4.134^{MD}$
$^4I_{11/2}$	962.7	1.18	0.267	0.261^{ED}
$^4I_{9/2}$	791.9	1.55	0.519	0.401^{ED}
$^4F_{9/2}$	650.9	3.22	1.595	1.674^{ED}
$^4S_{3/2}$	546.6	0.22	0.156	0.099^{ED}
$^2H_{11/2}$	516.9	10.6	8.369	8.146^{ED}
$^4F_{7/2}$	484.5	1.05	0.943	0.869^{ED}
$^2H_{9/2}$	407.3	0.39	0.505	0.486^{ED}
$^4G_{11/2}$	376.4	10.9	16.284	16.487^{ED}
$^4G_{9/2}$	363.4	0.81	1.288	1.304^{ED}
RMS dev.				*0.131*

‹λ› - "center of gravity" of the absorption band, Γ - integrated absorption coefficient, ED and MD stand for electric and magnetic dipole contributions, respectively (all values without superscript correspond to ED), RMS - root-mean-square deviation.

Table 3. Judd-Ofelt parameters Ω_k (k = 2, 4, 6) for Er^{3+}-doped fluoride crystals, oxyfluoride glass and GC.

Material	Ω_k, 10^{-20} cm^2			Ref.
	Ω_2	Ω_4	Ω_6	
Cs_2NaYF_6	0.665	0.217	0.029	This work
K_2YF_5	1.216	0.647	0.459	[32]
$NaYF_4$	1.65	0.56	1.01	[33]
$LiGdF_4$	0.905	2.47	4.92	[34]
BaY_2F_8	1.39	0.54	1.42	[35]
Er:BaF_2	1.048	1.478	1.009	[36]
CaF_2	1.043	0.866	1.725	[37]
LaF_3	1.27	0.28	0.63	[3]
glass	4.34	1.16	1.16	[38]
GC	1.68	7.70	1.34	[38]

Table 4. Emission probabilities for a 10 at.% Er^{3+}:Cs_2NaYF_6 crystal.

Transition		‹λ›, nm	$A_{JJ'}$, s^{-1}	$B_{JJ'}$, %	A_{tot}, s^{-1}	τ_{rad}, ms
$^4I_{13/2}\rightarrow$	$^4I_{15/2}$	1537	$2.46^{ED}+24.82^{MD}$	100.0	27.3	36.7
$^4I_{11/2}\rightarrow$	$^4I_{15/2}$	962.7	4.13^{ED}	46.9	8.8	113.4
	$^4I_{13/2}$	2576	$0.42^{ED}+4.26^{MD}$	53.1		
$^4I_{9/2}\rightarrow$	$^4I_{15/2}$	792.0	9.46^{ED}	69.4	13.6	73.3
	$^4I_{13/2}$	1634	3.48^{ED}	25.5		
	$^4I_{11/2}$	4467	$0.02^{ED}+0.67^{MD}$	5.1		
$^4F_{9/2}\rightarrow$	$^4I_{15/2}$	651.0	58.91^{ED}	86.0	68.5	14.6
	$^4I_{13/2}$	1129	3.5^{ED}	5.1		
	$^4I_{11/2}$	2010	$1.06^{ED}+3.49^{MD}$	6.6		
	$^4I_{9/2}$	3656	$0.18^{ED}+1.34^{MD}$	2.2		
$^4S_{3/2}\rightarrow$	$^4I_{15/2}$	546.6	4.93^{ED}	64.8	7.6	131.6
	$^4I_{13/2}$	848.2	2.02^{ED}	26.6		
	$^4I_{11/2}$	1265	0.18^{ED}	2.3		
	$^4I_{9/2}$	1764	0.48^{ED}	6.3		
$^2H_{11/2}\rightarrow$	$^4I_{15/2}$	516.9	518.02^{ED}	87.4	593	1.7
	$^4I_{13/2}$	778.8	$7.91^{ED}+49.43^{MD}$	9.7		
	$^4I_{11/2}$	1116	$4.73^{ED}+5.58^{MD}$	1.7		
	$^4I_{9/2}$	1488	$5.52^{ED}+0.49^{MD}$	1.0		
$^4F_{7/2}\rightarrow$	$^4I_{15/2}$	484.5	55.6^{ED}	51.7	107.6	9.3
	$^4I_{13/2}$	707.6	25.81^{ED}	24		
	$^4I_{11/2}$	975.5	8.43^{ED}	7.8		
	$^4I_{9/2}$	1248	$2.66^{ED}+7.80^{MD}$	9.7		
	$^4F_{9/2}$	1895	$0.24^{ED}+7.03^{MD}$	6.8		
$^4F_{5/2,3/2}\rightarrow$	$^4I_{15/2}$	449.3	0.82^{ED}	20.6	41.0	24.4
	$^4I_{13/2}$	634.8	7.74^{ED}	49.7		
	$^4I_{11/2}$	842.5	21.45^{ED}	11.9		
	$^4I_{9/2}$	1038	4.68^{ED}	7.3		
	$^4F_{9/2}$	1450	2.09^{ED}	4.9		
	$^4S_{3/2}$	2524	2.02^{ED}	5.2		
$^2H_{9/2}\rightarrow$	$^4I_{15/2}$	407.3	19.99^{ED}	11.9	20.4	49.1
	$^4I_{13/2}$	554.1	65.25^{ED}	38.9		
	$^4I_{11/2}$	705.9	$17.61^{ED}+27.62^{MD}$	27.0		
	$^4I_{9/2}$	838.3	$2.36^{ED}+0.55^{MD}$	1.7		
	$^4F_{9/2}$	1088	$1.08^{ED}+31.12^{MD}$	19.2		
$^4G_{11/2}\rightarrow$	$^4I_{15/2}$	376.4	1737^{ED}	53.8	167.7	5.9
	$^4I_{13/2}$	498.5	$135.22^{ED}+37.75^{MD}$	5.4		
	$^4F_{9/2}$	892.6	$50.3^{ED}+2.17^{MD}$	1.6		
$^4G_{9/2}\rightarrow$	$^4I_{15/2}$	363.4	148.63^{ED}	4.6	1737	0.31
	$^4I_{13/2}$	475.9	942.84^{ED}	29.2		
	$^4I_{11/2}$	583.7	58.85^{ED}	1.8		
	$^4F_{9/2}$	822.6	50^{ED}	1.5		

‹λ› - mean emission wavelength, $A_{JJ'}$ - probability of spontaneous transition (ED and MD stand for electric and magnetic dipole contributions, respectively; all values without superscript correspond to ED), $B_{JJ'}$ - luminescence branching ratio (only the transitions with $B_{JJ'} > 1\%$ are listed), A_{tot} - total probability of spontaneous transitions from the excited-state, τ_{rad} - radiative lifetime of excited-state.

Table 5 Radiative lifetimes τ_{rad} of the $^4I_{13/2}$ and $^4I_{11/2}$ excited-states for Er^{3+} ions in various crystals, oxyfluoride glass and GC (calculated with the J-O theory).

Crystal	$\tau_{rad}(^4I_{13/2})$, ms	$\tau_{rad}(^4I_{11/2})$, ms	Ref.
Cs_2NaYF_6	36.7	113.4	This work
K_2YF_5	14.89	17.39	[32]
YAG	7.3	8.8	[39]
YSGG	7.73	9.75	[40]
LaF_3	10.9	11.6	[3]
$NaYF_4$	16.2	11.8	[33]
BaY_2F_8	10.1	7.2	[35]
$LiYF_4$	10.0	6.7	[41]
glass	5.76	4.6	[38]
GC	5.40	4.6	[38]

Table 6 Evaluation of the non-radiative decay rates A_{NR} for a 0.3 at.% Er^{3+}:Cs_2NaYF_6 crystal.

State	ΔE_{min}, cm^{-1}	τ_{rad}, ms	τ_{exp}, ms	$A_{NR} = 1/\tau_{exp} - 1/\tau_{rad}$, s^{-1}
$^4I_{15/2}$				
$^4I_{13/2}$	6506	36.7	34.5	1.3
$^4I_{11/2}$	3889	113.4	14.1	62.1
$^4I_{9/2}$	2231	73.3	0.030	33319.7
$^4F_{9/2}$	2734	14.6	0.165	5992.1
$^4S_{3/2}$	2955	131.6	0.120	8325.7

ΔE_{min} - energy-gap to the next lower-lying state (calculated between the state barycenters), τ_{rad} - radiative lifetime of the excited-state (calculated with the J-O theory), τ_{exp} - experimental lifetime.

Table 7 Constants describing the non-radiative relaxation, C and α, for fluoride crystals.

Crystal	α, 10^{-3} cm	C, 10^7 s^{-1}	ν_{max}, cm^{-1}	Ref.
Cs_2NaYF_6	2.78	1.31	450-500	This work
K_2YF_5	2.77	0.85	418	[32]
LaF_3	5.3-6.0	314-355	350	[3]
$LiYF_4$	3.6-3.8	3.5-6.7	560-580	[47]
MnF_2	4.5	187	350	[49]
SrF_2	4.5	31	360	[50]
BaY_2F_8	4.1	4.5	390	[51]